

# MELT QUALITY OF A356.2 ALLOY IN THE PRESSURE COUNTER PRESSURE CASTING PROCESS FOR STEERING KNUCKLES

Libing Liu , Yunhu Zhang and Changjiang Song

Center for Advanced Solidification Technology (CAST), School of Materials Science and Engineering, Shanghai University, Shanghai 200444, China

Wenbin Zhou and Feng Liu

Shanghai Huizhong Automotive Manufacturing Co., Ltd. (SHAC), 1493 South Pudong Road, Shanghai 200122, China

Gordon H. Peters

66 Industrial Service Company Ltd. E00D, 28 Hristo Botev str./blvd. Triaditsa Distr., Fl. 4, 1000 Sofia, Bulgaria

Copyright © 2023 American Foundry Society  
<https://doi.org/10.1007/s40962-023-01079-6>

## Abstract

*The present study investigates the melt quality of A356.2 alloy during the pressure counter pressure casting (CPC) process for steering knuckles, by means of fracture analysis of tensile test bars, hydrogen content measurement, and inclusion analysis. The failure modes of the tensile test bars suggest that oxides are the most detrimental inclusions in the CPC cast A356.2-T6 steering knuckles. Hydrogen content at various stages is quantified using the HYCAL analysis apparatus, revealing a sharp decrease to  $0.16 \pm 0.01$  ml/100 g after degassing, followed by a slight increase in the holding and CPC process. The porous disc filtration apparatus (PoDFA) method is employed to identify different types of inclusions, including  $TiB_2$ ,  $Al_4C_3$ ,  $\alpha-Al_2O_3$ , spinel-like, spinel, oxide films, and  $MgO$ . The content of different inclusions analysis indicates that*

*oxides can be effectively removed during degassing, but can easily re-form as the melt moves up and down in the riser tubes. The characteristics of the molten bath and the mechanism of slag formation in different CPC cycles are discussed, which provides a comprehensive understanding of the increase in oxide size and concentration from the first to the last casting cycle. This increase leads to a deterioration of the melt quality as well as the casting quality. It is thus essential to minimize oxidation and limit the liquid front velocity to ensure the consistent production of high-integrity castings in the CPC process.*

**Keywords:** A356.2 alloy, melt quality, CPC, PoDFA, hydrogen, inclusions

## Introduction

A356.2 with T6 heat treatment is the most frequently used low-pressure cast aluminum alloy for automotive load-bearing components due to its favorable properties, including good casting, machining, weldability, qualified mechanical properties, as well as significant weight savings.<sup>1-3</sup> However, high-volume production of A356.2 alloy necessitates consistent and adequate melt quality to ensure the desired casting integrity.<sup>4-6</sup> In low-pressure casting (LPC) plants, it is a common practice to mix a substantial

fraction of scrap castings or secondary ingots with primary ingots in the melting process.<sup>7,8</sup> This practice can increase the inclusion content in the molten metal.<sup>9</sup> Inclusions are typically detrimental to the mechanical properties of castings and can lead to premature failure of components and tensile test bars.<sup>4</sup> Therefore, it is crucial to closely monitor and control the melt quality to ensure that the casting integrity of A356.2 alloy is maintained at a high level during the production process.

Inclusions in the A356.2 melt can be classified as exogenous and endogenous. Exogenous inclusions include the shedding of refractories, graphite, and grain refiner particles. Aluminum oxide ( $Al_2O_3$ ) as particles or biofilms,<sup>10</sup>

aluminum carbide ( $\text{Al}_4\text{C}_3$ ), magnesium oxide ( $\text{MgO}$ ), and spinel ( $\text{MgAl}_2\text{O}_4$ ) are endogenous inclusions.<sup>11,12</sup> Various techniques have been developed to detect inclusions in aluminum melts, including the reduced pressure test, K-mold, liquid metal cleanliness analyzer, PoDFA, and its successor PREFIL. PoDFA is a quantitative technique to identify the types and contents of inclusions in the melt,<sup>13–15</sup> it involves filtering a certain quantity of liquid aluminum through a very fine filter (pore size at about 10–100  $\mu\text{m}$ ) disc under specific conditions. Inclusions are concentrated at the filter interface by a factor of 10,000 thus their types and content can be identified.<sup>12,16</sup>

The CPC process, an advancement of LPC,<sup>17,18</sup> is extensively utilized for producing safety components for automobiles that require greater strength and ductility compared to those made by LPC and gravity casting techniques.<sup>19</sup> Therefore, the mechanical properties of castings fabricated using the CPC process are typically more demanding. The original equipment manufacturer (OEM) specified ultimate tensile strength (UTS) and total elongation (TE) requirements for A356.2-T6 steering knuckles manufactured by CPC average of 315 MPa and 8% for three samples, respectively, with a minimum of 305 MPa and 6%.<sup>19,20</sup> Despite this, tensile test bars sometimes fail prematurely during routine testing, and metal cleanliness is a significant challenge encountered by foundry technician during the CPC process.<sup>7</sup> Therefore, the effect of inclusions and hydrogen on mechanical property degradation is a major concern. Maintaining metal quality in molten aluminum alloys necessitates the monitoring and minimization of the presence of inclusions and hydrogen. While RPT and K-mold techniques are utilized in casting plants to assess melt cleanliness, they lack the necessary accuracy. Thus, the quantitative analysis of melt quality in A356.2 alloy at different steps of the CPC process should be considered.

This paper investigates the melt quality of A356.2-T6 steering knuckles produced by the CPC process, with a particular focus on the evolution of inclusions and hydrogen content. Specifically, the study collects tensile test bars that failed to meet UTS or TE requirements and performs fracture analysis to identify premature failure modes caused by inclusions. Additionally, hydrogen content measurement and PoDFA analysis are conducted at different steps of the CPC process to understand the evolution of melt quality. The study also analyzes the types and contents of different inclusions present at different stages. Finally, the paper discusses the characteristics of the molten bath and the mechanism of slag formation in various CPC cycles, providing valuable insight into the increase in oxide size and concentration over multiple casting cycles.

## Melt Quality Assessment Procedures

### Assessment Methods

#### *Tensile Test Bars Containing Inclusions*

In this study, prematurely failed tensile test bars from routine testing of several Volkswagen steering knuckles at SHAC's foundry were utilized to analyze inclusions. The test bar sampling position varied for different products, and the DIN 50125 standard was employed for the tensile test procedure, using type A test bars with a diameter ( $d_0$ ) of 5 mm and a gauge length of 25 mm. After slicing the T6 heat-treated steering knuckles, the test bars were turned and then tested at room temperature with a strain rate of  $6.7 \times 10^{-3}/\text{s}$ . A total of 30 bars with prominent inclusions on their fracture surfaces were analyzed to investigate the detrimental effects of inclusions. The proportion of unqualified test bars was calculated as 3.1% (30 out of 968 tested bars).

#### *Hydrogen Content Measurement*

The concentration of hydrogen at various stages was determined using the HYCAL hydrogen analysis apparatus, as illustrated in Figure 1a. The apparatus employs field-proven probe and closed-loop recirculation technologies, enabling fast online quantitative measurement of dissolved hydrogen. To measure the hydrogen content, the hydrogen detection probe was placed at a distance of 15 to 30 cm from the surface of the molten aluminum and away from any vertical wall, and the working principle is shown in Figure 1b. The final result was obtained within 5–10 min for each batch.

#### *PoDFA Test*

The PoDFA apparatus and schematic diagram of the sample analysis process are given in Figures 2a and b. For each PoDFA sample, around 2.5 kg of molten metal is taken from a location that is 20 cm beneath the liquid melt surface and positioned away from any vertical wall. It was assumed that the inclusions and oxides present beneath the surface of the liquid melt could serve as representative indicators of the melt quality at different stages of the process. In order to ensure consistent and accurate results, the ladle used in the PoDFA test must be preheated for a minimum of five minutes in the liquid melt and any surface dross must be removed before each test. The filtration crucible assembled with a filter should be preheated for about 30 min in the crucible heater to minimize heat losses during the transfer of the liquid metal. Once the filtered

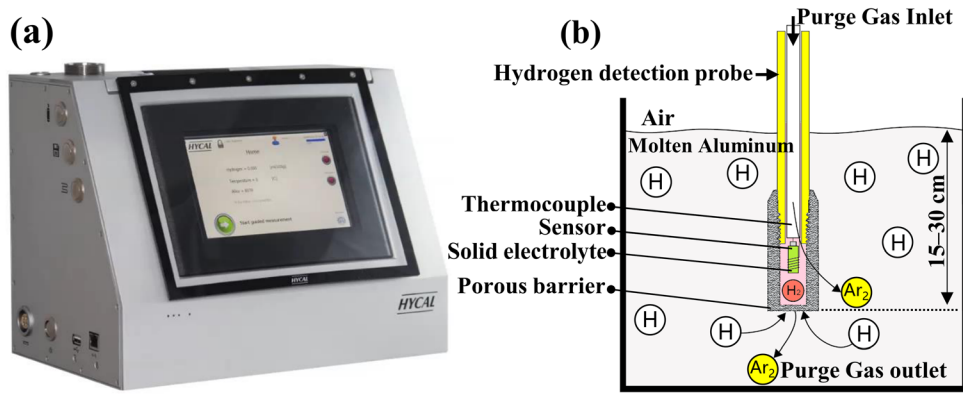


Figure 1. (a) HYCAL hydrogen analysis apparatus and (b) the working principle.

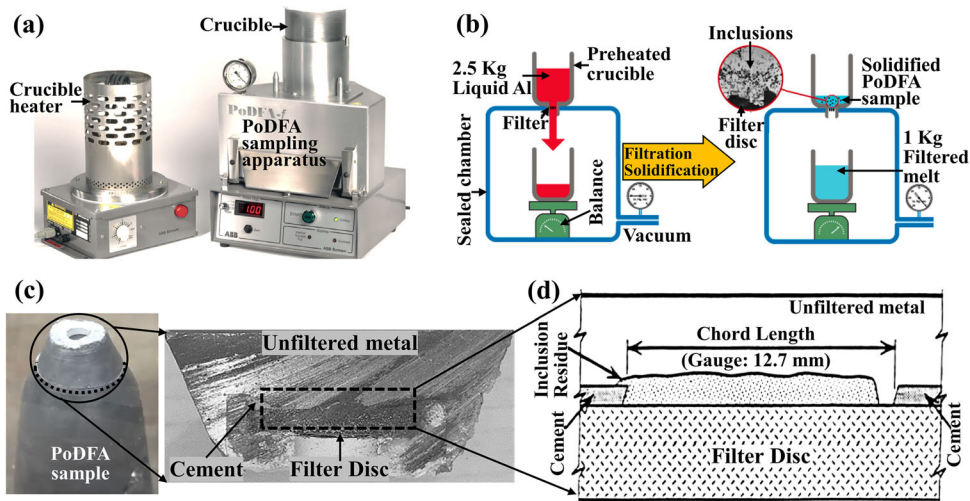


Figure 2. (a) PoDFA apparatus photos are courtesy of Alcan Inc.; (b) Schematic diagram of the PoDFA sampling process; (c) PoDFA sample cutting; (d) Schematic diagram of the area to be analyzed.

melt on the balance has reached the desired weight of 1 kg, the PoDFA filtration process will automatically cease and the residual melt in the filtration crucible will solidify in the air. The resulting solidified metal and filter, which forms a conical sample as depicted in Figure 2c, are cut, mounted, and polished prior to microscopic observation. A schematic diagram of the area to be analyzed at the PoDFA filter cake interface is presented in Figure 2d, where the

Zeiss AXIO IMAGER A2M) is used to analyze PoDFA samples after mechanical polishing, scanning electron microscope (SEM, 20 kV, JSM6480) with an Inca Energy Dispersive Spectrometry (EDS) is used to analyze the inclusion types and size.

Total index inclusions ( $\text{mm}^2/\text{Kg}$ )=

$$\frac{\text{Total number of square measured} \times \text{Factor of correction} \times \text{Nominal chord}(12.7 \text{ mm})}{\text{Filtered weight}(\text{Kg}) \times \text{Chord length measured}(\text{mm})}$$

inclusion content can be quantified by means of image analysis of the concentrated inclusions from the fine filter interface. The grid method is employed to classify the inclusions and determine the total inclusion content.<sup>21</sup> Optical microscope (OM, Zeiss Axiovert 40 MAT, and

The correction factor used in the analysis is dependent on the magnification of the microscope and is set at 0.01, 0.0025, or 0.000625 for magnifications of 50 X, 100 X, or 200 X, respectively.

## Assessment Locations

In the SHAC's foundry, the primary ingots, scrap castings, and secondary ingots (with a maximum percentage of (scrap + secondary)/total  $\leq 50\%$ ) are melted at approximately 760 °C using a natural gas furnace. The liquid melt is then transferred through the launder to a holding furnace, which is a resistance furnace with a theoretical capacity of 900 kg. The holding furnace can maintain a stable temperature range of 725–740 °C at the degassing station and the CPC casting cell, with 75% of its theoretical capacity functional. The rotary degassing process involves a cleaning flux of 0.7 kg per ton, an argon flow of 40 L/min, a rotation speed of 500 rpm, and a duration of 15 min at  $730 \pm 10$  °C. During the degassing process, the melt is grain-refined using an Al-5Ti-B rod (target addition 0.08 wt%) and modified using an Al-10Sr rod (target addition 0.1 wt%). The CPC process employs dry compressed air, and the dew point of the air is monitored using a moisture separator. In each casting cycle, a fiberglass filter is placed on the sprue area of each cavity, in addition to the preheating cycle. In this study, the hydrogen content and PoDFA tests are conducted throughout the path of molten metal processing.

Figure 3 shows the molten metal process path of A356.2 alloy, including the steps for PoDFA sampling and hydrogen detection. The objective of this study is to comprehensively evaluate the melt quality evolution throughout the entire CPC process under diverse conditions, the situation where the molten metal remains at the degassing station for 2 hours following degassing is also considered. The first PoDFA sample (a) is obtained from the molten pool of the natural gas furnace, while the remaining PoDFA samples (b, c, d, e, f) are collected from the same holding furnace at different stages in the same trial. In total, six sets of PoDFA samples are taken

throughout the entire molten metal process path. To minimize the impact of fluctuations in the sampling process, at least three consecutive trials are conducted for each set of PoDFA samples. Furthermore, the hydrogen content at different locations is detected, with a minimum of three detection trials carried out for each location. Notably, the hydrogen content of the casting (middle) position is not detected due to the sealed holding furnace under the CPC cell during casting.

The A356.2 alloy composition is analyzed at various locations using an optical emission spectrometer (SPECTRO), and the results are presented in Table 1. The addition of Al-5Ti-B and Al-10Sr master alloys during degassing causes a slight increase in Ti, B, and Sr concentrations compared to the step after refilling. The presence of residual aluminum liquid in the holding furnace before refilling allows for the detection of Sr at this step. Additionally, magnesium is added during degassing. The composition of the melt remains stable throughout the holding process until the end of casting.

## Results

### Premature Failure Modes of Tensile Test Bars

The representative fracture morphologies of test bars are shown in Figure 4. The corresponding UTS and TE are marked on each image. The results indicate that TE is more sensitive to inclusions than UTS, as all test bars exhibiting premature failure exhibited unqualified TE. The chemical compositions of points (a), (b), and (c) in Figure 4 are listed in Table 2. From the magnified image of Figure 4(a<sub>1</sub>) and EDS data, inclusions containing O, Mg, Sr, K, and Ca elements were observed with a size larger than 100  $\mu\text{m}$ . These inclusions may be attributed to the presence of Al–Sr

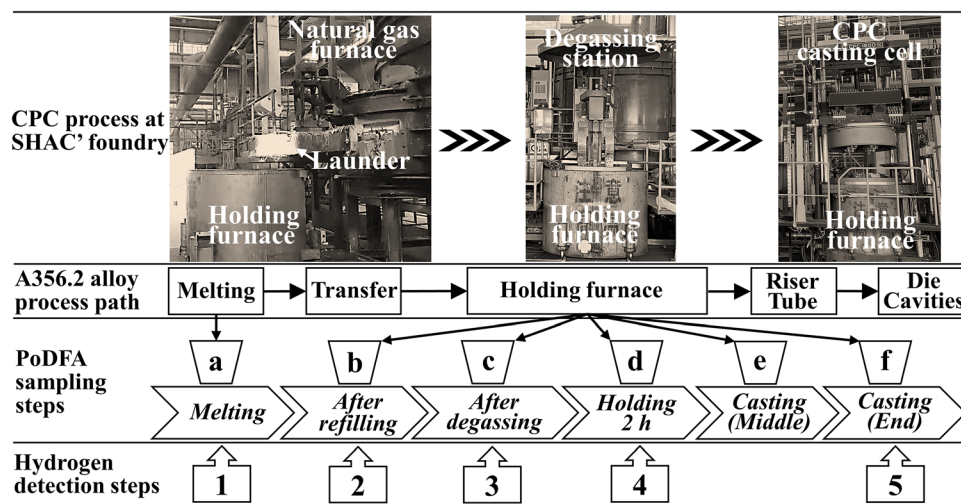
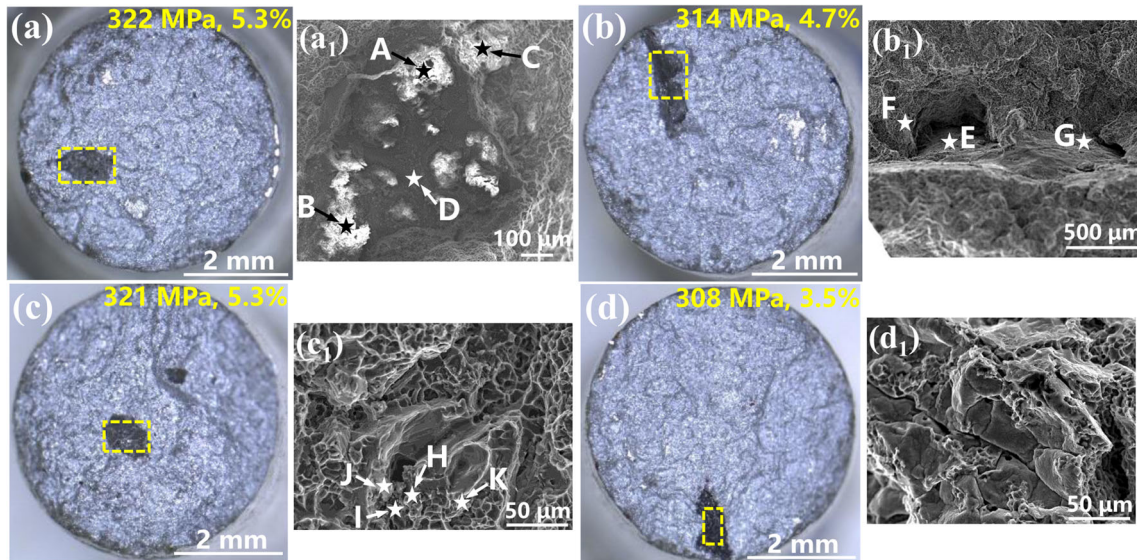


Figure 3. CPC process at SHAC's foundry, molten metal process path of A356.2 alloy, PoDFA sampling and hydrogen detection steps.

**Table 1. A356.2 Alloy Composition at Different Locations**

Requirements (wt%)	Al Balance	Si 6.5–7.5	Fe ≤0.15	Cu ≤0.03	Mn ≤0.1	Mg 0.3–0.45	Ti 0.08–0.25	B –	Sr –
After refilling	92.4	6.97	0.118	0.002	0.004	0.358	0.126	0.0001	0.007
After degassing	92.5	6.85	0.116	0.002	0.004	0.389	0.132	0.0006	0.014
Holding 2 h	92.5	6.81	0.116	0.002	0.004	0.395	0.134	0.0005	0.014
Casting (End)	92.5	6.81	0.117	0.002	0.004	0.388	0.130	0.0005	0.014



**Figure 4. The representative fracture morphologies of tensile test bars with premature failure.**

**Table 2. The Element Content of Points in Figure 4a, b, and c**

Element (wt%)	C	O	Mg	Al	Si	Ti	Fe	Sr	Cl	K	Ca
A	15.9	27.6	13.4	8.3	–	–	–	31.5	0.6	1.7	1.1
B	17.4	27.6	12.4	8.4	–	–	–	31.8	–	1.3	1.2
C	–	26.2	16.7	57.2	–	–	–	–	–	–	–
D	14.1	24.9	18.0	24.2	–	–	–	18.8	–	–	–
E	22.0	7.1	1.8	55.4	31.5	–	–	–	–	–	–
F	11.9	–	0.7	68.1	19.3	–	–	–	–	–	–
G	20.1	–	1.4	74.8	3.5	–	–	–	–	–	–
H	–	21.4	8.0	57.5	7.3	2.0	3.8	–	–	–	–
I	–	5.8	2.5	70.8	12.5	4.8	3.6	–	–	–	–
J	13.7	30.7	1.3	48.3	6.0	–	–	–	–	–	–
K	–	–	–	63.6	15.7	–	20.7	–	–	–	–

and fluxing additions during degassing, leading to the agglomeration of their oxides and subsequent flow into the casting. As shown in Figure 4b, shrinkage pores with high Si content defects resulted in a TE of 4.7%. In addition, Ti and Fe-containing compounds were identified in Figure 4c. Figure 4d shows the folded oxide film, also known as

bifilms,<sup>9</sup> leading to a TE of only 3.5%. Typically, bifilms form on the melt surface during entrainment, and have only a few milliseconds to grow before submersion.<sup>22</sup>

By analyzing the different types of defects on the fractures, the failure modes of the tensile test bars with premature

failure can be obtained. As shown in Figure 5, they can be classified by the following categories: oxides, carbides, chlorides and borides, and porosity. The total number of defects analyzed among the 30 test bars was 43. Among them, 65.1% of defects are oxides with a size range of 100–2000  $\mu\text{m}$ . The proportion of carbides is 16.3%, which has a size range of 50–300  $\mu\text{m}$ . Other defects are chlorides and borides, porosity, both of which account for 9.3 percent. Based on these observations, it can be inferred that oxides represent the most hazardous inclusions in A356.2-T6 steering knuckles manufactured by the CPC process.

## Hydrogen Content

During the aluminum melt processing, interactions of hydrogen absorption and oxide film formation on the surface are critical.<sup>23</sup> Moreover, the hydrogen content is associated with inclusions because it increases with the

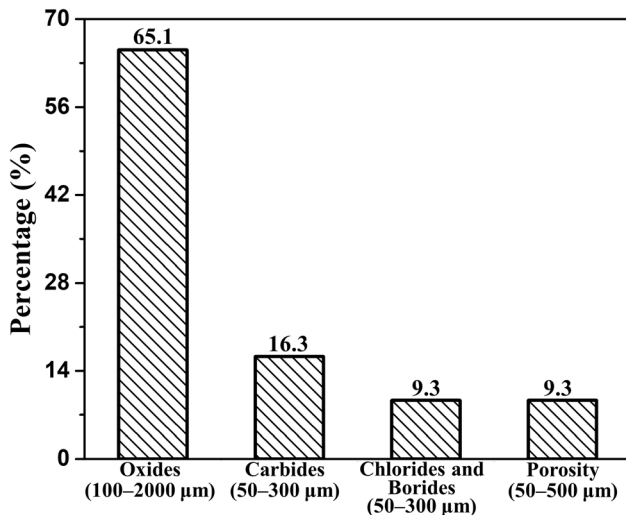


Figure 5. Failure modes in tension test bars with premature failure.

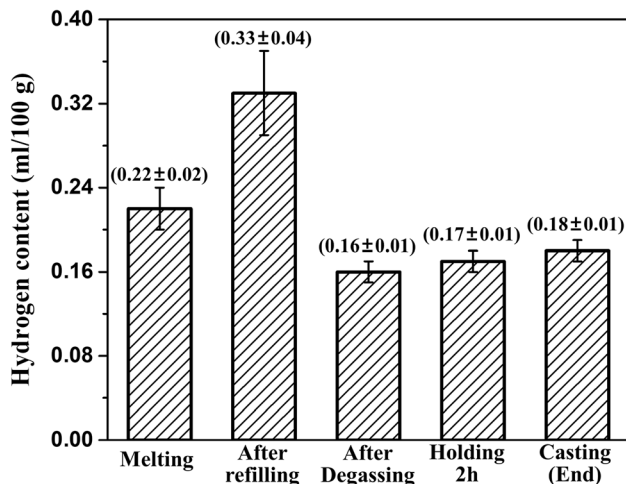


Figure 6. Hydrogen content at different steps.

increase of inclusion content at a certain temperature.<sup>5,24</sup>

Hydrogen content at different steps during the CPC process is detected by the HYCAL hydrogen analysis apparatus, which is given in Figure 6. The hydrogen content is  $0.22 \pm 0.02$  ml/100 g in the melting procedure. Subsequently, the hydrogen content significantly increased to  $0.33 \pm 0.04$  ml/100 g after the melt was transferred into the holding furnace, which could be caused by the high pour height that brings entrainment hydrogen during the melt transfer.<sup>23</sup> Initially, the pour height from the launder bottom to the melt surface in the holding furnace was approximately 100 cm and decreased to approximately 30 cm ultimately. The hydrogen content dropped sharply to  $0.16 \pm 0.01$  ml/100 g after degassing, indicating that the efficiency of degassing is roughly 50%. Finally, the hydrogen content marginally increased to  $0.17 \pm 0.01$  ml/100 g after being held for 2 h at 730  $^{\circ}\text{C}$  in the holding furnace, and  $0.18 \pm 0.01$  ml/100 g at the CPC casting end.

## Inclusion Types

The representative collages of the whole PoDFA filter cake interface at different steps are shown in Figure 7. They provide an overall picture of the melt quality in the CPC process. In the melting stage, inclusions are distributed throughout the residual metal rather than agglomerated at the filter interface, as shown in Figure 7a. However, after refilling, a significant number of inclusions agglomerate at the filter interface, as depicted in Figure 7b. Subsequently, the agglomerated inclusions are scarcely observed in the residual metal after degassing and holding for 2 h. During the CPC casting, inclusions appear to have increased significantly. A number of inclusions at the filter interface can be found in the casting middle. Moreover, the inclusion content appears to rise during the subsequent CPC process stages until the casting end, with more inclusions visible in Figure 7f than in Figure 7e.

Most of the inclusions in A356.2 can be identified in the optical micrograph analysis, and the key residue micrographs are given in Figure 8.  $\text{TiB}_2$ ,  $\text{Al}_4\text{C}_3$ ,  $\alpha\text{-Al}_2\text{O}_3$ , spinel-like, spinel, and oxide films are the main inclusions that are marked on these images. In the melting furnace, spinel and spinel-like particles are the most common inclusions which can be easily observed. After refilling, all kinds of inclusions with a size range of 10–100  $\mu\text{m}$  can be found. The size and content of the inclusions are significantly reduced after degassing and at the subsequent holding for 2 h, which can be verified in Figures 8c and d. As previously mentioned, the size and content of the inclusions increased significantly during the CPC casting. There are a lot of intermetallic phases generated at these two steps according to the micrographs in Figure 8e and f, which causes the inclusions to appear significantly increased.

To understand all different types of inclusions in A356.2 alloy during the CPC process, SEM analysis of PoDFA

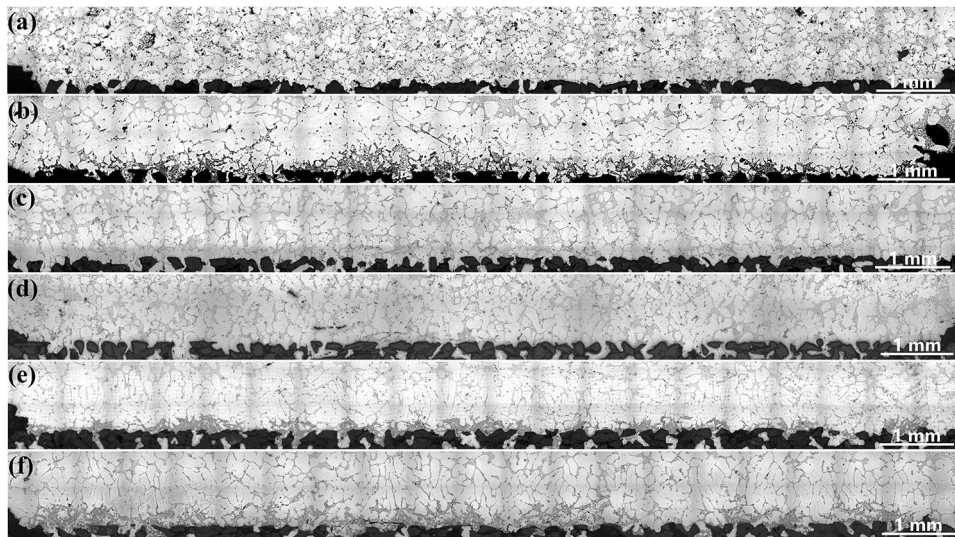


**Figure 7. Collages of the whole filter cake of PoDFA samples at different steps: (a) Melting; (b) After refilling; (c) After degassing; (d) Holding-2h; (e) Casting middle; (f) Casting end.**

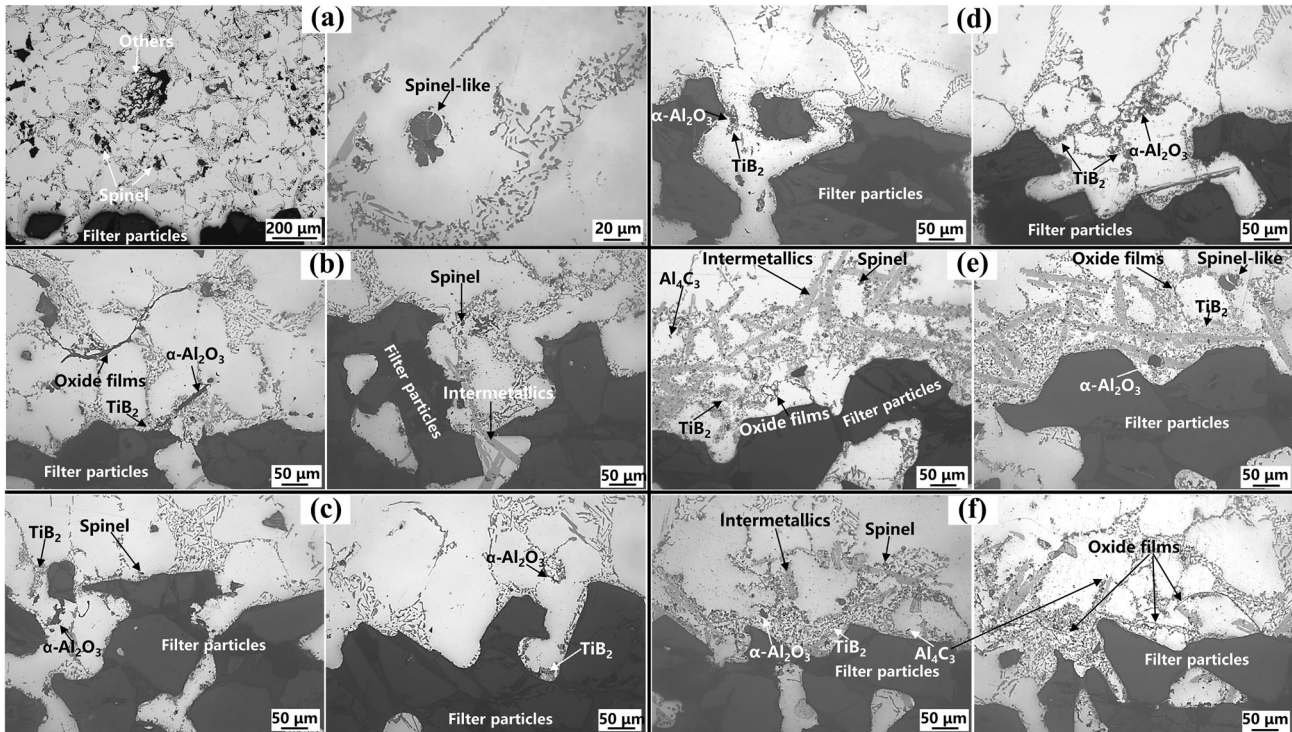


**Figure 8. Micrographs of inclusions at different steps: (a) Melting; (b) After refilling; (c) After degassing; (d) Holding-2h; (e) Casting middle; (f) Casting end.**

samples in the melting furnace and the casting end were conducted. EDS maps confirmed the presence of MgO agglomerations combined with oxide films in Figure 9a, suggesting that these MgO particles are entrapped by oxide films and subsequently submerged in the bulk liquid, leading to their irregular shapes.<sup>25</sup> The (TiV)B<sub>2</sub> agglomerations with tens of microns were detected in Figure 9b, which may originate from the process of boron treatment to remove impurity elements but are not settled during

smelting.<sup>26</sup> The observation of oxide films with trapped MgO particles in Figure 9b highlights the issue of Mg oxidation during the melting process. Although the oxidation of Mg is considerable in A356.2 alloy, the size of the individual MgO particle is typically smaller than 3 μm (see the inserted image of Figure 9b), making it challenging to quantify them via OM in PoDFA test. Therefore, it is necessary to detect the Mg content during the degassing step to ensure it meets the product requirements.

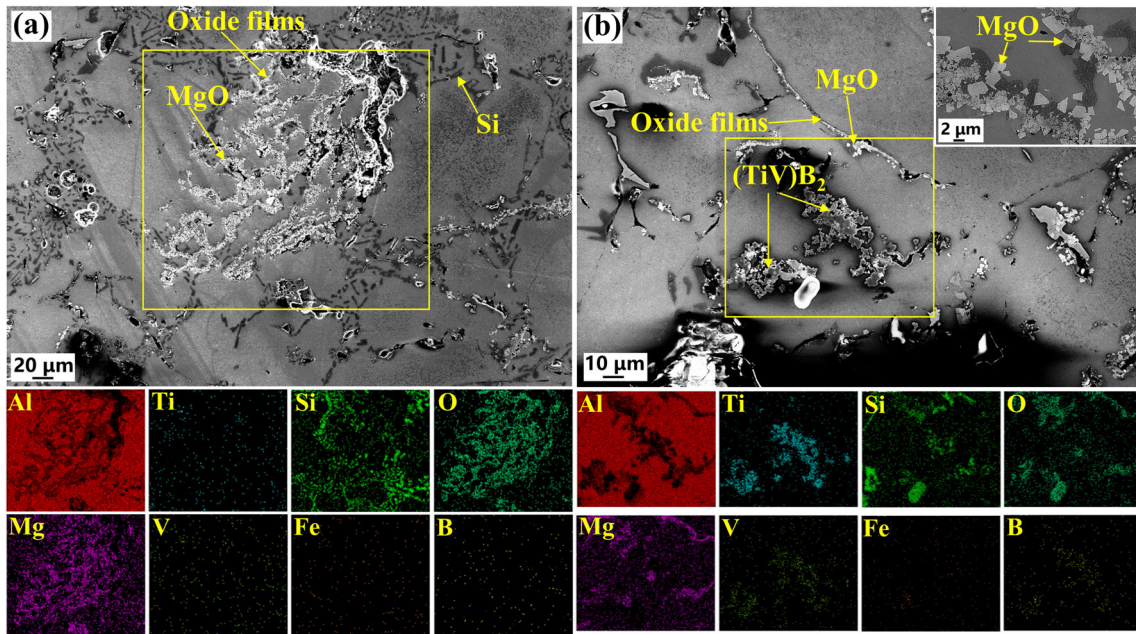


Figure 9. SEM micrographs of inclusions and EDS maps of PoDFA sample in the melting furnace: (a) and (b) are different areas of the sample.

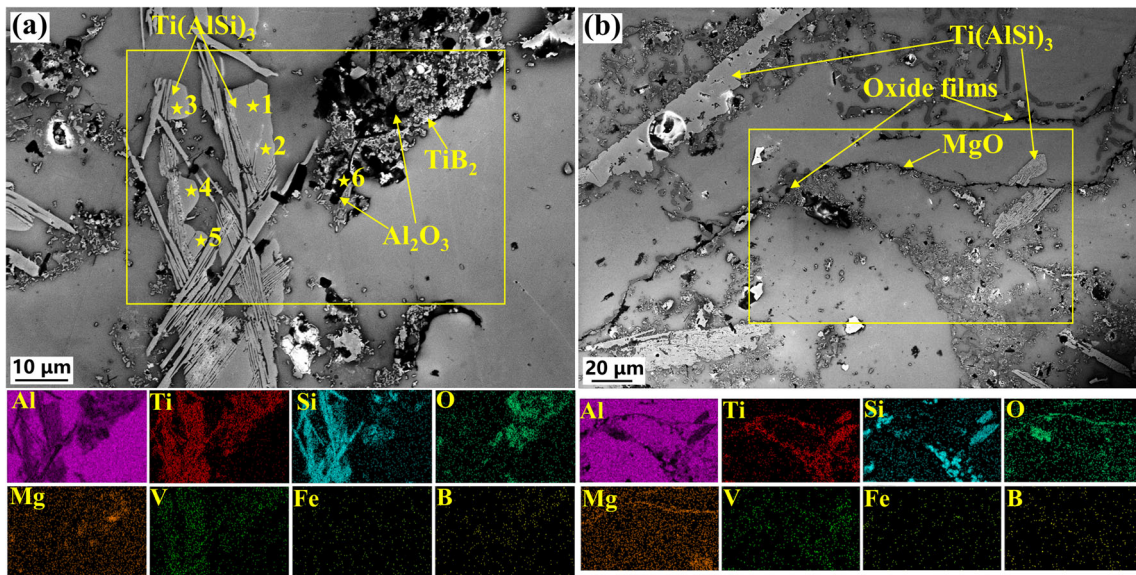


Figure 10. SEM micrographs of inclusions, EDS point and maps of PoDFA sample in the casting end: (a) and (b) are different areas of the sample.

SEM analysis of PoDFA sample at the casting end are shown in Figure 10, and the corresponding element content of points in Figure 10a is listed in Table 3. The EDS data confirm that the intermetallic phases observed in Figure 8b, e and f are composed of  $Ti(AlSi)_3$ , which exhibits a flake-like morphology. The formation of  $Ti(AlSi)_3$  is attributed to the excess of Ti in A356.2 beyond the solubility limit of 0.1 wt%,<sup>27,28</sup> the actual Ti content in the present alloy is 0.13 wt% according to Table 1, and slow cooling condition during PoDFA

solidification may produce flakes morphology of  $Ti(AlSi)_3$ .<sup>29</sup> Furthermore, prolonged holding of a melt with a Ti content exceeding 0.1 wt% is prone to the formation of  $Ti(AlSi)_3$  sludge at the bottom of the crucible, adversely affecting the foundry processes and the properties of the final castings.<sup>30</sup> Various other types of inclusions, such as  $Al_2O_3$ ,  $TiB_2$ ,  $MgO$  are also present at the casting end, which may serve as substrates for nucleation of  $Ti(AlSi)_3$  and lead to agglomeration of more inclusions at the filter interface.



## The Content of Different Inclusions

It is vital to identify all sorts of inclusions as well as the content, thereby the quality of the A356.2 melt can be obtained in the CPC process. The total inclusions and oxide

**Table 3. Element Content of Points in Figure 9a**

Element (at.%)	Al	Ti	Si	O	Mg	V	Fe
1	63.7	23.8	11.8	0	0.1	0.5	0
2	64.0	23.8	11.7	0	0.1	0.4	0.1
3	62.9	23.9	12.6	0	0.1	0.6	0
4	63.7	23.5	12.2	0	0	0.5	0.1
5	61.6	22.8	15.0	0	0	0.6	0
6	33.6	3.1	11.9	50.1	0.3	0	0

films detected by PoDFA method are given in Figure 11a. The total inclusions content is less than 0.9 mm<sup>2</sup>/kg at different steps, it even increased after degassing operation because of the deliberately added grain refining TiB<sub>2</sub> particles. The content of TiB<sub>2</sub> increased by an average of 0.35 mm<sup>2</sup>/kg after degassing from the histogram in Figure 11b. The settling effect during the 2-h holding period reduced the total inclusions content. Furthermore, inclusions and oxides are formed in the riser tube as the melt washes up and down in every cycle of the CPC casting,<sup>22</sup> so they both increased in the casting middle and casting end. The trend of the oxide films content is consistent with the total inclusions, the number of oxide films increased after degasser is due to an excess of turbulence in the holding furnace. The histogram in Figure 11c gives the Al<sub>4</sub>C<sub>3</sub> contents at different steps, it seems that Al<sub>4</sub>C<sub>3</sub> is not sensitive to the degassing operation, its content is increased slightly after degassing and then maintained at a

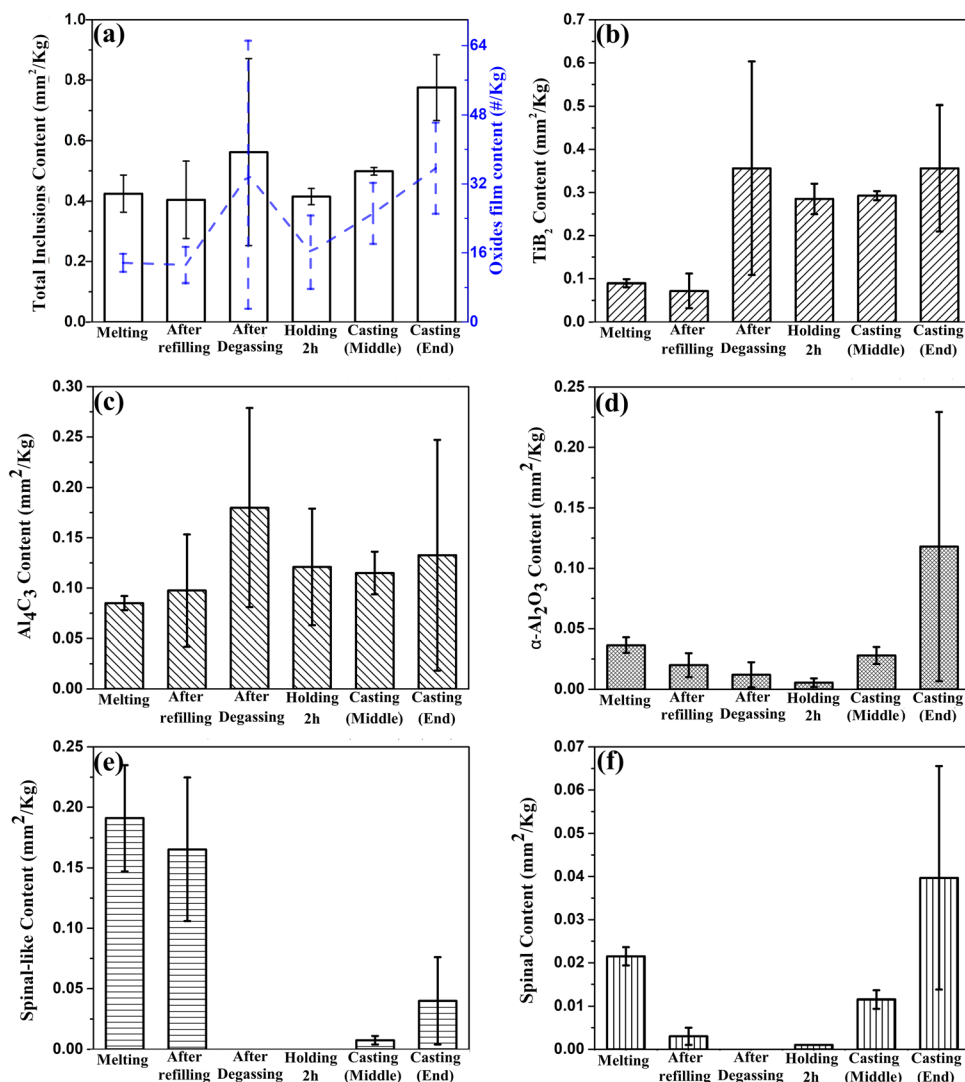


**Figure 11. The content of different inclusions in A356.2 alloy at different steps of CPC process: (a) Total inclusions and oxide films; (b) TiB<sub>2</sub>; (c) Al<sub>4</sub>C<sub>3</sub>; (d) α-Al<sub>2</sub>O<sub>3</sub>; (e) Spinel-like; (f) Spinel-MgAl<sub>2</sub>O<sub>4</sub>.**

stable level of  $0.12 \text{ mm}^2/\text{kg}$ . Although a considerable amount of  $\text{TiB}_2$  and  $\text{Al}_4\text{C}_3$  were found in the melt, they were not considered harmful because they were in good atomic contact with the Al matrix and did not initiate other defects such as pores and cracks.<sup>25</sup>

The content of  $\alpha\text{-Al}_2\text{O}_3$ , spinel-like, and spinel are given in Figure 11d, e, and f, respectively. These inclusions are mainly formed due to oxidation and can be effectively removed during the degassing process according to the histograms. However, these oxides can regenerate in each CPC cycle and accumulate in the residual melt of the holding furnace. The content of  $\alpha\text{-Al}_2\text{O}_3$  reaches  $0.12 \pm 0.11 \text{ mm}^2/\text{kg}$  at the casting end. This explains why their content increased in the casting middle and casting end. Additionally, during each CPC cycle, the melt in the riser tube falls down when the pressure is released in the holding furnace, and the 'whoosh' effect in the bottom of the furnace stirs the oxide sediments and other inclusions back into suspension. Consequently, these inclusions are easily reintroduced in the subsequent casting cycle.<sup>22</sup> As mentioned earlier, the presence of oxides poses a significant risk to the casting quality and can cause premature failure of tensile test bars. The lack of bonding between oxide films is prone to induce cracks in the casting, making them a critical factor to be addressed in the CPC process.<sup>31</sup>

## Discussion

### The Characteristics of Molten Bath in Different CPC Cycles

The results of the PoDFA analysis revealed a significant increase in the concentration of oxides (including oxide films) during the CPC cycles, suggesting their increased likelihood of being entrained during casting. Furthermore, oxides have been identified as the most detrimental inclusions in the premature failure of tensile test bars. Campbell has highlighted the dangers associated with double, unbonded oxide films, also known as bifilms.<sup>10</sup> He suggested that bifilms are practically universally present in metals, there seems mounting evidence that the bifilms usually cause cracks, and their presence can be used to explain many aspects of failure behaviors by fracture and corrosion.<sup>10</sup> Bifilms possess a distinctive feature of having an internal non-bonded surface but perfect exterior wetting in the melt. Additionally, they serve as preferred substrates for the nucleation and growth of other inclusions, leading to an overall increase in the total inclusions during the CPC cycles.

In order to produce high-integrity castings, it is crucial to comprehend the characteristics of the molten bath at various stages of different CPC cycles. The core parts of a CPC cell include a sealed mold mounted above a sealed furnace filled with liquid A356.2. The characteristics of liquid

A356.2 in different CPC casting cycles are illustrated in Figure 12. Figure 12(a<sub>1</sub>) shows the pressurization stage in the first cycle with a full crucible, the related components and different factors are marked. Pressurization of the sealed chamber and holding furnace is accomplished by utilizing dry compressed air. The melt flows up via riser tubes to the cavities by applying higher pressure in the holding furnace than in the chamber. This allows the melt fills into the casting cavity at a controlled and tranquil rate under countering pressure. However, during this process, the oxide film on the melt surface thickens due to the unavoidable contact of the melt surface with vapor and oxygen. At this stage, convection in the melt predominantly occurs from the crucible bottom to the riser tube nozzle. Table 4 provides the densities of different phases in liquid Al, with denser inclusions settling and agglomerating into sediments at the crucible bottom. Meanwhile, the Brownian motion of inclusion particles remains ongoing in the molten bath. As the filling proceeds, the melt surface in the crucible gradually falls until the cavities are all fully filled. Figure 12(a<sub>2</sub>) shows the pressure release stage in the first cycle, the castings in each cavity are almost solidified. The height of the melt in the riser tube is  $H_1$  before pressure release, and the melt drops back into the furnace instantly after the pressure release. Consequently, the sediments at the crucible bottom may wash back into the melt, and the  $H_1$  provides energy for the convection in the opposite direction compared to the pressurization stage. Figure 12(a<sub>3</sub>) shows the parts extracted stage in the first cycle, where there is no forced convection in the molten bath at this stage, and the settling may be pronounced. Upon opening the sealed chamber, air enters all cavities above the liquid surface of the inner riser tube. The vapor and oxygen in the air may interact with the Al-wetted inner riser tube surface, leading to the formation of a layer of oxide film. In a CPC casting cycle, the melt is transferred into the mold uphill against gravity, with the sideways movement of the surface film likely resulting in its becoming the skin of the riser tube, and oxide films forming in the riser tube as the melt washes up and down.<sup>22</sup>

Figure 12(b<sub>1</sub>–b<sub>3</sub>) illustrates the behavior of the molten bath in the last cycle with minimum melt in the crucible. Owing to the smaller volume of the molten bath and a greater consumption of melt required to fill the riser tube, convection in this cycle is more intense compared to the first cycle. Thus inclusions that are suspended in the melt can easily enter into the casting. The highest height ( $H_2$  in Figure 12b<sub>2</sub>) of the melt in the fill tube causes intense convection after pressure release, which may lead to minimum sediments at the bottom of the holding furnace. It is worth noting that the Brownian motion and settling of particles persist throughout all cycles. Figure 12(b<sub>3</sub>) shows the extracted stage in the last cycle, indicating the completion of the CPC casting of molten A356.2 in the removable holding furnace is over.

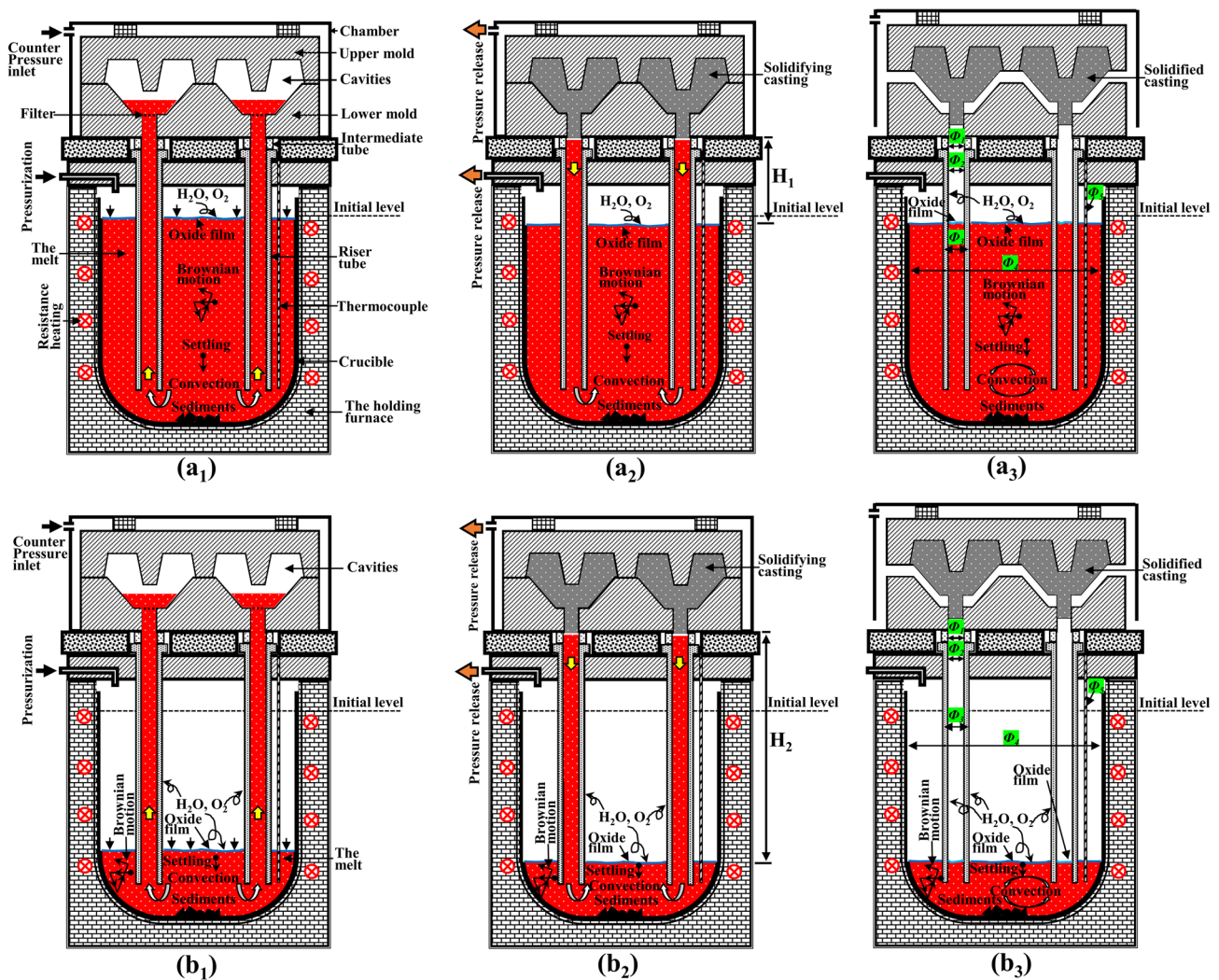


**Figure 12. Schematic diagram of characteristics of the molten bath in different CPC casting cycles: (a<sub>1</sub>) The pressurization stage in the first cycle with a full crucible; (a<sub>2</sub>) The pressure release stage in the first cycle; (a<sub>3</sub>) The parts extracted stage in the first cycle; (b<sub>1</sub>) The pressurization stage in the last cycle with minimum melt in the crucible; (b<sub>2</sub>) The pressure release stage in the last cycle; (b<sub>3</sub>) The parts extracted stage in the last cycle.**

**Table 4. The Density of Different Phases in Liquid Al<sup>32,33</sup>**

Phase	Liquid Al	Graphite	Chlorides	Al <sub>2</sub> O <sub>3</sub>	MgAl <sub>2</sub> O <sub>4</sub>	MgO	Al <sub>4</sub> C <sub>3</sub>	TiB <sub>2</sub>
Density (g/cm <sup>3</sup> )	2.3–2.5	2.09–2.23	1.98–2.16	3.97	3.60	3.58	2.36	4.51

### The Slag Formation on the Vertical Surfaces

In general, the holding furnace in the CPC cell must be refilled periodically as the melt is consumed during the casting process, and the weight of castings determines how many parts can be produced before the furnace must be replenished. As the melt in the furnace is depleted with each cycle, the volume in the sealed furnace that needs to be pressurized and the height that the molten metal must travel to reach the mold both increase. These two factors must be taken into account to ensure consistent filling of the casting mold. Although a programmable logic

controller (PLC) compensation factor is already implemented to ensure that the molten metal front reaches the mold at the same time for different casting cycles.<sup>17</sup> The variations in the molten metal quality and the formation of slag from the first to the last cycle should also be taken into consideration.

Figure 13a and b present the mechanisms of slag formation on the vertical surfaces in contact with liquid Al. Meanwhile, Figure 14 displays images of the resulting slag formations on the vertical surfaces in contact with liquid Al in the foundry. It is worth noting that a notable deposition

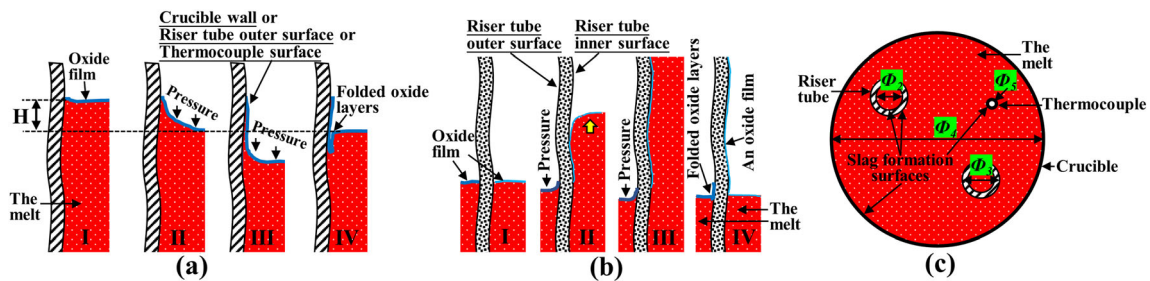


**Figure 13. (a) Slag formation mechanism on the crucible wall, riser tube outer surface and thermocouple surface; (b) Slag formation mechanism on the riser tube inner surface; (c) Cross-section view of the holding furnace.**

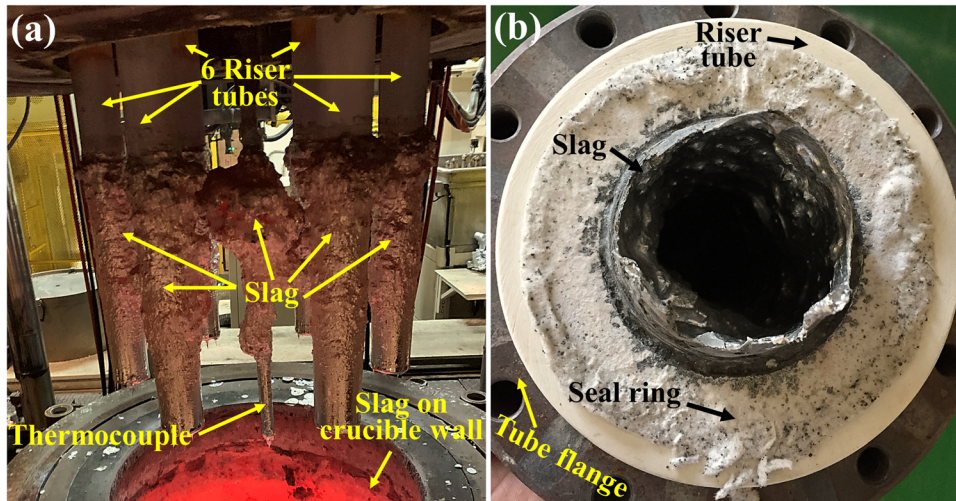


**Figure 14. Images of slag formation on the vertical surfaces in contact with liquid Al in the CPC process: (a) slag on the crucible wall, riser tube outer surface, and thermocouple surface; (b) slag on the riser tube inner surface.**

of slag, spanning a few centimeters, is observed on both the riser tubes and thermocouple. The accumulation period for the slag on the thermocouple amounts to approximately 2 months, while for the inner and outer surfaces of the riser tubes, the accumulation time extends to approximately two weeks. The appropriate management and handling of these slag accumulations are of utmost importance in preserving the quality of the melt in subsequent crucible operations. The slag formation process can be segmented into four stages, as depicted in Figure 13a and b, wherein the liquid surfaces inside and outside the riser tube are distinguished.

**Stage I:** The liquid levels inside and outside the riser tube remain constant, and an oxide film forms on the surfaces of these two areas, the sealed holding furnace remains unpressurized in this stage;

**Stage II:** A higher pressure is applied to the holding furnace than to the chamber, causing the melt surface in the crucible to drop, and the oxide film in contact with the vertical wall becomes caught and stretched by the falling melt surface. Meanwhile, the surface inside the riser tube rises, and most of the films inside the riser tube become torn and trapped by the tube wall.;

**Stage III:** The pressure in the sealed furnace reaches its maximum, and the melt surface in the crucible drops to its lowest level. The oxide films become attached to the crucible wall, riser tube outer surface, and thermocouple surface. The films trapped by the riser tube's inner wall will not melt into liquid Al even if the tube is filled with molten metal;

**Stage IV:** The pressure is released in the sealed furnace, and the melt in the riser tube drops back into the crucible, causing the melt surface in the crucible to rise to a certain height compared to the lowest level in Stage III. Simultaneously, the oxide film folds along the vertical surface with the rising surface, and the Al-wetted riser tube's inner surface oxidizes until the next filling. The liquid surface ultimately drops H in a casting cycle.

The slag formation process on the vertical surfaces in a casting cycle can be well explained by these stages, with the folding-in of oxide films on the vertical wall being a recurring feature in each cycle. As the casting operation progresses, the accumulation of oxide films on these vertical surfaces takes place in a layer-by-layer fashion, as evidenced by the images presented in Figure 14. The cross-

section view of the holding furnace, as presented in Figure 13(c), facilitates the calculation of the cross-sectional area of the melt in the crucible, which can be expressed as  $S = \pi * (\Phi_4^2 - n\Phi_3^2 + n\Phi_2^2 - \Phi_5^2) / 4$ . Here,  $\Phi_2$  is the inside diameter of the riser tube,  $\Phi_3$  is the outside diameter of the riser tube,  $\Phi_4$  is the inside diameter of the crucible,  $\Phi_5$  is the diameter of the thermocouple protective shell,  $n$  is the number of riser tubes. Theoretically,  $S$  should remain constant to ensure the consistency of  $H$  across all casting cycles for a specific casting. This is imperative to enable the appropriate functioning of the compensation factor employed in the filling profile. Nevertheless, as evidenced by Figure 14, a significant amount of slag accumulates on the riser tube and thermocouple, leading to changes in  $S$  and ultimately resulting in the alteration of  $H$ . If  $H$  becomes a variable, the preset compensation parameters will be invalid so a tranquil mold filling in the CPC process cannot be guaranteed. Thus, many entrained defects will appear in the products.

The characteristics of the molten bath and the slag formation process in different CPC cycles suggest that oxidation can generate a significant number of bifilms in the melt, leading to a significant deterioration of the final casting quality. This, in turn, can diminish the advantage of the CPC process to produce high-integrity components. To prevent the formation of bifilms, it is essential to maintain an oxidation-free melt and ensure that the surface of the liquid metal does not fold over on itself.<sup>9,10,22,25</sup> Compressed nitrogen, which should be substantially free of particulates, oil, and moisture, can be used as an economic substitute for compressed dry air to avoid oxidation issues. Additionally, by controlling the liquid front velocity to not exceed the critical value (0.5 m/s for liquid aluminum), the potential of entrained surface films can be significantly reduced or eliminated.<sup>10,34</sup> An effective furnace cleaning and riser tube and thermocouple protection tube cleaning or maintenance program is critical to reducing slag accumulation. Another good practice is the use of a disposable filter screen that is placed just above the sprue before each cycle,<sup>17</sup> the metal flow also tends to be less turbulent.<sup>35</sup> By implementing these actions, the hazards of the oxide film will be minimized in the CPC process.

## Conclusions

In this paper, the melt quality of A356.2 alloy in the CPC process has been assessed in multiple ways. The characteristics of the molten bath and the slag formation on the vertical surfaces in different CPC cycles have been discussed. Conclusions can be drawn as follows:

- (1) The fracture analysis of tensile test bars revealed that 65.1% of defects in A356.2-T6 steering knuckles manufactured by the CPC process are oxides with a size range of 100–2000  $\mu\text{m}$ , which are considered the most hazardous inclusions.

- (2) The hydrogen content in the melt can reach  $0.33 \pm 0.04$  ml/100 g before degassing, and the efficiency of degassing is approximately 50%. The hydrogen content slowly increases during holding for 2 h and subsequent CPC casting.
- (3) Different types of inclusions, including  $\text{TiB}_2$ ,  $\text{Al}_4\text{C}_3$ ,  $\alpha\text{-Al}_2\text{O}_3$ , spinel-like, spinel, oxide films, and  $\text{MgO}$ , were identified by PoDFA and SEM.  $\text{TiB}_2$  and  $\text{Al}_4\text{C}_3$  were not considered harmful as they were in good atomic contact with the Al matrix.  $\alpha\text{-Al}_2\text{O}_3$ , spinel-like, and spinel can be removed effectively during degassing but are regenerated in the CPC casting due to oxidation. The content of  $\alpha\text{-Al}_2\text{O}_3$  increased to  $0.12 \pm 0.11$  mm<sup>2</sup>/kg at the casting end.
- (4) Oxide films are easily formed in the melt riser tube as liquid aluminum washes up and down, causing the oxides content to keep increasing, and the size of oxides to become fairly large. This leads to a significant amount of slag accumulation on the vertical surfaces from the first to the last CPC cycle.
- (5) Oxidation in the CPC cycles can cause a substantial deterioration of the melt quality and casting integrity. Thus, it is critical to ensure that the melt is oxidation-free as much as possible, and the liquid front velocity does not exceed the critical value to ensure high-integrity castings are consistently produced.

## Acknowledgments

This work was financially supported by the National Natural Science Foundation of China (51974183 and 51974184), Gao pin zhi zai sheng lv gui xi he jin zhi zao gong yi ji shi fan ying yong (2022FRD05007) and the Natural Science Foundation of Shanghai (22ZR1425000). The authors would like to express their sincere thanks to the Technical Center of SHAC.

## REFERENCES

1. P.N. Anyalebechi, G. Rapids, Effect of process route on the structure, tensile, and fatigue properties of aluminum alloy automotive steering knuckles. *Int. Foundry Res.* **12** (2011)
2. S. Otarawanna, A.K. Dahle, Casting of aluminium alloys. In *Fundamentals of Aluminium Metallurgy* 2011, pp. 141–154. <https://doi.org/10.1533/9780857090256.1.141>
3. C.M. Sonsino, R. Franz, Multiaxial fatigue assessment for automotive safety components of cast aluminium EN AC-42000 T6 (G-AlSi7Mg0.3 T6) under constant and variable amplitude loading. *Int. J. Fatigue* (2017). <https://doi.org/10.1016/j.ijfatigue.2016.10.027>

4. M. Brůna, A. Sládek, Hydrogen analysis and effect of filtration on final quality of castings from aluminium alloy AlSi7Mg0.3. *Arch. Foundry Eng.* **11**(1), 6 (2011)
5. D. Dispinar, J. Campbell, A comparison of methods used to assess aluminium melt quality, in *TMS Annual Meeting*, p. 8 (2007)
6. M. Riestra, A. Bjurenstedt, T. Bogdanoff et al., Complexities in the assessment of melt quality. *Int. J. Metalcast.* **12**, 441–448 (2018). <https://doi.org/10.1007/s40962-017-0179-y>
7. J. Wannasin, D. Schwam, J.F. Wallace, Evaluation of methods for metal cleanliness assessment in die casting. *J. Mater. Process. Technol.* (2007). <https://doi.org/10.1016/j.jmatprotec.2007.03.013>
8. C. Yuksel, O. Tamer, E. Erzi, U. Aybarc, E. Cubuklusu, O. Topcuoglu, M. Cigdem, D. Dispinar, Quality evaluation of remelted A356 scraps. *Arch. Foundry Eng.* (2016). <https://doi.org/10.1515/afe-2016-0069>
9. R. Gopalan, N.K. Prabhu, Oxide bifilms in aluminium alloy castings—a review. *Mater. Sci. Technol.* (2013). <https://doi.org/10.1179/1743284711Y.0000000033>
10. J. Campbell, The consolidation of metals: the origin of bifilms. *J. Mater. Sci.* **51**(1), 96–106 (2015). <https://doi.org/10.1007/s10853-015-9399-9>
11. M. Jolly, Prof. John Campbell's ten rules for making reliable castings. *Jom* (2005). <https://doi.org/10.1007/s11837-005-0091-4>
12. L. Liu, F.H. Samuel, Assessment of melt cleanliness in A356.2 aluminium casting alloy using the porous disc filtration apparatus technique: part I Inclusion measurements. *J. Mater. Sci.* (1997). <https://doi.org/10.1023/A:1018602725185>
13. D. Doutré, B. Gariépy, J.P. Martin, G. Dubé, Aluminium Cleanliness: Methods and Applications in Process Development and Quality Control, *Light Metals 17* (1985)
14. M.B. Djurdjević, Z. Odanović, J. Pavlović-Krstić, Melt Quality control at aluminum casting plants, Association of Metallurgical Engineers of Serbia (2010). <https://www.dykast.com/user/products/4329-pdfs-2-file.pdf>
15. M. Gökelma, J. Morscheiser, M. Badowski, T. Dang, P. Le Brun, S. Tewes, Observation on inclusion settling by LiMCA and PoDFA analysis in aluminium melts. *Int. Alum. J.* **91**, 6 (2015)
16. P.G. Enright, I.R. Hughes, J. Pickering, A. Simard, J. Proulx, Characterisation of molten metal quality using the pressure filtration. *Trans. Am. Foundry Soc.* **111**, 193–203 (2003)
17. G.G. Woycik, G. Peters, *Low-Pressure Metal Casting, Casting, Vol 15, ASM Handbook*, ed. by S. Viswanathan, D. Apelian, R.J. Donahue, B. DasGupta, M. Gywn, J.L. Jorstad, R.W. Monroe, M. Sahoo, T.E. Prucha, D. Twarog, (ASM International, 2008), pp. 700–708. <https://doi.org/10.31399/asm.hb.v15.a0005261>
18. T.E. Prucha, Metal mold processes-gravity and low pressure technology. *AFS International Conference on Structural Aluminum Casting*. SAC, Nov 2003, pp. 119–136 (2003)
19. G. Ruff, T.E. Prucha, J. Barry, D. Patterson, Pressure counter pressure casting (PCPC) for automotive aluminum structural components. *SAE Trans.* **110**, 360–365 (2001)
20. A. Maneva, S. Stanev, M. Georguiev, L. Nenova, Comparative study of mechanical properties and structure of knuckles intended for application in the running gear of automotive. *Int. J. "NDT Days"* **IV**(5), 9 (2021)
21. P.V. Evans, P.G. Enright, R.A. Ricks, Molten Metal Cleanliness: Recent Developments to Improve Measurement Reliability, *Light Metals* (2018), pp. 839–846. [https://doi.org/10.1007/978-3-319-72284-9\\_109](https://doi.org/10.1007/978-3-319-72284-9_109)
22. J. Campbell, Stop pouring, start casting. *Int. J. Metalcast.* (2015). <https://doi.org/10.1007/BF03355529>
23. D. Dispinar, J. Campbell, Critical assessment of reduced pressure test. Part 1: porosity phenomena. *Int. J. Cast Met. Res.* (2004). <https://doi.org/10.1179/136404604225020696>
24. D. Lapham, C. Schwandt, M. Hills, R. Kumar, D.J.I. Fray, The detection of hydrogen in molten aluminium. *Ionics* (2002). <https://doi.org/10.1007/BF02376052>
25. J. Campbell, *Complete Casting Handbook. Metal Casting Processes, Techniques and Design*, (Elsevier Science, 2011), pp. 3–103
26. G.G. Gauthier, The conductivity of super-purity aluminium: the influence of small metallic additions. *J. Inst. Met* **59**, 22 (1936)
27. D.G. McCartney, Grain refining of aluminium and its alloys using inoculants. *Int. Mater. Rev.* (1989). <https://doi.org/10.1179/imr.1989.34.1.247>
28. X.G. Chen, M. Fortier, TiAlSi intermetallic formation and its impact on the casting processing in Al–Si alloys. *J. Mater. Proc. Technol.* (2010). <https://doi.org/10.1016/j.jmatprotec.2010.06.009>
29. X. Chen, M. Fortier, Formation of primary TiAlSi intermetallic compounds in Al-Si foundry alloys. *Mater. Forum.* 659–665 (2004). <http://www.icaa-conference.net/ICAA9/data/papers/GP%2090.pdf>
30. G.K. Sigworth, T.A. Kuhn, Grain refinement of aluminum casting alloys. *Int. J. Metalcast* **1**, 31–40 (2007). <https://doi.org/10.1007/BF03355416>
31. C. Nayhumwa, N.R. Green, J. Campbell, Influence of casting technique and hot isostatic pressing on the fatigue of an Al-7Si-Mg alloy. *Metall. Mater. Trans. A* (2001). <https://doi.org/10.1007/s11661-001-0266-8>
32. R. Peterson, Common impurities in aluminum alloys, in *Proceedings of 3rd International Conference on Aluminum Processing*, Paris, 1994, pp. 75–89

33. Y. Plevachuk, V. Sklyarchuk, A. Yakymovych, S. Eckert, B. Willers, K. Eigenfeld, Density, viscosity, and electrical conductivity of hypoeutectic Al-Cu liquid alloys. *Metall. Mater. Trans. A* **39**(12), 3040–3045 (2008). <https://doi.org/10.1007/s11661-008-9659-2>
34. J. Campbell, Entrainment defects. *Mater. Sci. Technol.* (2006). <https://doi.org/10.1179/174328406X74248>
35. L.N.W. Damoah, L. Zhang, Removal of inclusions from aluminum through filtration. *Metall. Mater. Trans. B* (2010). <https://doi.org/10.1007/s11663-010-9367-3>

**Publisher's Note** Springer Nature remains neutral with regard to jurisdictional claims in published maps and institutional affiliations.

Springer Nature or its licensor (e.g. a society or other partner) holds exclusive rights to this article under a publishing agreement with the author(s) or other rightsholder(s); author self-archiving of the accepted manuscript version of this article is solely governed by the terms of such publishing agreement and applicable law.